

# Topological quantum critical points in the extended Bose-Hubbard model

Joana Fraxanet,<sup>1</sup> Daniel González-Cuadra,<sup>1</sup> Tilman Pfau,<sup>2</sup> Maciej Lewenstein,<sup>1,3</sup> Tim Langen,<sup>2</sup> and Luca Barbiero<sup>1</sup>

<sup>1</sup>ICFO - Institut de Ciències Fotòniques, The Barcelona Institute of Science and Technology, 08860 Castelldefels (Barcelona), Spain

<sup>2</sup>5. Physikalisches Institut and Center for Integrated Quantum Science and Technology, Universität Stuttgart, Pfaffenwaldring 57, 70569 Stuttgart, Germany

<sup>3</sup>ICREA, Pg. Lluís Companys 23, ES-08010 Barcelona, Spain

(Dated: June 30, 2021)

The combination of topology and quantum criticality can give rise to an exotic mix of counterintuitive effects. Here, we show that unexpected topological properties take place in a paradigmatic strongly-correlated Hamiltonian: the 1D extended Bose-Hubbard model. In particular, we reveal the presence of two distinct topological quantum critical points with localized edge states and gapless bulk excitations. Our results show that the topological critical points separate two phases, one topologically protected and the other topologically trivial, both characterized by a long-range ordered string correlation function. The long-range order persists also at the topological critical points and it reflects the presence of localized edge states protected by a finite charge gap. Finally, we introduce a super-resolution quantum gas microscopy scheme for dipolar dysprosium atoms, which provides a reliable route towards the experimental study of topological quantum critical points.

*Introduction* Topology represents a fascinating and challenging topic in different areas of modern quantum physics [1–3]. Among the related interesting quantum phenomena one can find conducting edge modes in bulk gapped phases [4, 5], quantized conductance [6–9] and, fractionalized charges [10–12]. At the same time, due to the gapped and non-local nature of their elementary excitations, topological phases represent a particularly suitable platform, where fault-tolerant quantum computation could be performed [13–17].

While in non-interacting systems [18] symmetry arguments allow for a complete description of topological insulators [19–21] and superconductors [22], the study of topology in many-body quantum systems represents a more challenging task [23]. In this context, the notion of symmetry-protected topological (SPT) phases [24–27] has allowed to classify different strongly-correlated quantum states that are topologically protected only up to local perturbations preserving specific symmetries. Celebrated examples of such fully gapped topological states of matter are the Haldane phase occurring in several strongly correlated systems [28–43], and the topological Mott insulator (TMI) appearing in interacting Su-Schrieffer-Heger (SSH) models [44–51]. Noticeably, the impressive level of flexibility and accuracy reachable in ultracold atomic platforms has allowed for the experimental realizations of these SPT phases [52, 53].

Interestingly, recent works have shown that, contrary to the standard intuition, topology can also occur in critical phases [27, 54–66]. In this direction, special attention has to be paid when dealing with topological phase transitions. As shown in specific models [64], topologically protected edge states can remain localized at critical points despite the presence of gapless bulk excitations. Due to the novelty of the concept of topological quantum critical points (TQCPs), aspects related to the mechanism that protects the topology are not yet fully understood.

The results reported in this paper provide a ground for a better comprehension of TQCPs. Our analysis, based on density-matrix-renormalization-group (DMRG) [67–69] calculations, indeed shows that these states of matter occur in very distinct regimes of the broadly investigated one dimensional ex-

tended Bose-Hubbard model (EBHM). Here, we unveil that, for large enough density-density interaction, different TQCPs take place both at unit density and at half filling in the presence of a lattice dimerization. Despite the usual vanishing bulk gap at quantum criticality, our results show that here the topology can remain protected by a finite charge gap. This scenario holds in quantum critical points separating two phases, one topological and the other trivial, which share a similar type of long-range order captured by the same string correlation function. This hypothesis is confirmed by studying other topological phase transitions between phases not having a similar magnetic ordering. There, we find that both the bulk and the charge gap vanish and, as expected, the topological properties disappear.

In order to present a reliable route to probe the existence of TQCPs, we provide a detailed scheme involving magnetic atoms with dipolar long-range interaction [70]. The role of such atoms is becoming even more fundamental thanks to the recent achievements related to droplets physics [71, 72], thermalization [73], supersolidity [74–76], topological pumping [77] and, most notably, the implementation of the EBHM [78]. However, the dipolar interaction in current experimental setups has been too weak to explore the full EBHM phase diagram. Here, we propose a new quantum gas microscopy scheme based on strongly-interacting dysprosium atoms trapped in a short wavelength optical lattice. As we show, this choice allows us to make precise predictions about the experimental realization and detection of TQCPs.

*Model.* The considered Hamiltonian is the 1D extended Bose-Hubbard model

$$H = - \sum_{i=1}^{L-1} (J + \delta J(-1)^i) (b_i^\dagger b_{i+1} + \text{h.c.}) + \frac{U}{2} \sum_{i=1}^L n_i(n_i - 1) + V \sum_{i=1}^{L-1} n_i n_{i+1}, \quad (1)$$

where  $b_i^\dagger (b_i)$  is the bosonic operator describing the creation (annihilation) of a particle at the  $i$ -site of a lattice of length  $L$  filled with  $N$  bosons. The bosonic tunneling amplitude

$J - \delta J (J + \delta J)$  describes hopping processes in odd (even) links connecting two nearest-neighbor (NN) sites while  $U$  and  $V$  represent, respectively, the onsite and NN interactions. The most investigated version of eq. (1) is the homogeneous case  $\delta J = 0$  at unit density  $\bar{n} = N/L = 1$ . Here, early studies [79, 80] discovered the presence of three different phases: a gapless superfluid in the limit of weak interaction, a Mott insulator (MI) in the regime of strong onsite repulsion and, for large enough  $V$ , a charge density wave (CDW<sub>1</sub>) with effective local antiferromagnetic order between pairs and empty sites. More recently [30], it has been demonstrated that in the regime of intermediate couplings a fully gapped SPT phase with non-local antiferromagnetic order between pairs and empty sites can occur. The latter corresponds to the celebrated Haldane insulator (HI), originally discovered in spin-1 chains [28]. On the other hand, eq. (1) at  $\delta J > 0$  has been only partially investigated [81, 82]. At  $\bar{n} = 1/2$ , the strongly repulsive regime unveils the presence of a phase transition between a topological Mott insulator (TMI) having the same non-trivial topological features of SSH chains [83], and a charge density wave (CDW<sub>1/2</sub>) with local antiferromagnetic order signaled by alternated empty and single occupied sites. Although the gapped topological phases in eq. (1) are properly understood, the study of possible topological states appearing at quantum critical points remains an open challenge that we tackle in the following paragraphs.

*Homogeneous case ( $\delta J = 0$ ) at  $\bar{n} = 1$ .* SPT phases are characterized by two main features: degenerate localized edge states and gapped bulk excitations. The first requirement can be tested by looking at the behavior of the edge localization length  $\xi_e$ , which can be extracted from the relation  $|E_+ - E_-| \sim e^{-L/\xi_e}$ . Here,  $E_{\pm}$  are the energies of the two degenerate ground states,  $|L\rangle \pm |R\rangle$ , where  $|L\rangle(|R\rangle)$  denotes a state with the left (right) edge state occupied by a bosonic pair and the right (left) edge state empty [85]. In particular, a thermodynamic extrapolation is expected to show  $\xi_e^{-1} \neq 0$  in the presence of localized edge states and  $\xi_e^{-1} \rightarrow 0$  as they delocalize and become bulk states. Analogously, gapped bulk excitations are captured by a finite value of the bulk correlation length  $\xi_b \sim \Delta E_{bulk}^{-1}$ , where  $\Delta E_{bulk} = E_1 - E_{GS}$  is the lowest energy bulk gap and  $E_{GS}$  ( $E_1$ ) is the energy of the ground (first excited) state. As usual, at quantum criticality  $\Delta E_{bulk} = 0$ , therefore a diverging  $\xi_b$  is expected. In Fig. 1(a-b), our DMRG calculations show that the HI has all the aforementioned features, namely  $\xi_e^{-1}, \xi_b^{-1} \neq 0$ . At the same time, the SPT nature of HI demands uniquely non-local order parameters to probe such a regime. More specifically, the non-local order parameters describing the HI are  $\mathcal{O}_{1,\alpha}(j) = e^{i\pi \sum_{k<j} S_1^\alpha(k)} S_1^\alpha(j)$ , where  $\alpha = x, z$  and  $S_1^x(i) = \frac{1}{\sqrt{2}} \left( \sqrt{1 - \frac{n_i}{2}} b_i + b_i^\dagger \sqrt{1 - \frac{n_i}{2}} \right)$  and  $S_1^z(i) = 1 - n_i$  [34]. The HI is therefore characterized by the long-range order of the string correlation functions

$$\mathcal{O}_{1,\alpha}^2(|i-j|) = \langle \mathcal{O}_{1,\alpha}(i) \mathcal{O}_{1,\alpha}(j) \rangle, \quad \alpha = x, z. \quad (2)$$

Due to the absence of effective rotational  $x \leftrightarrow z$  symmetry in the model eq. (1), the two correlators  $\mathcal{O}_{1,\alpha}^2$  are expected to behave very differently in CDW<sub>1</sub>. In particular, the local an-

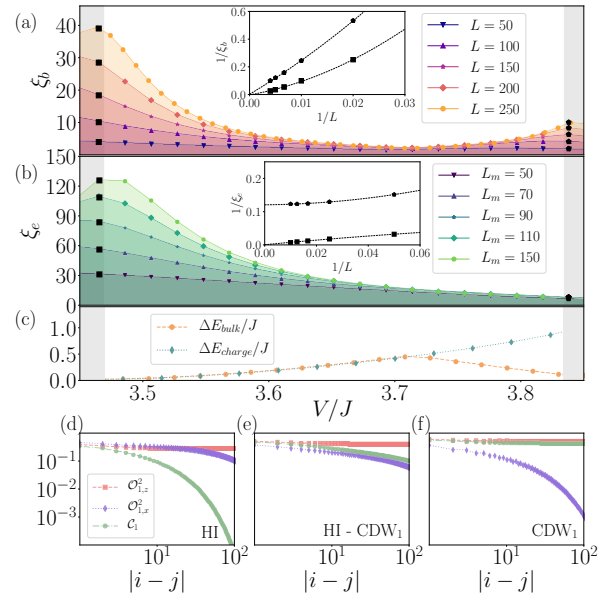


Figure 1. Edge  $\xi_e$  (a) and bulk  $\xi_b$  (b) correlation length in units of the lattice spacing  $a_{lat}$ , obtained by DMRG simulations of the model in eq. (1) with  $\bar{n} = 1$ ,  $\delta J = 0$ ,  $U/J = 6$  as a function of  $V/J$ . The insets refer to the finite size extrapolation of  $\xi_e$  and  $\xi_b$  at the MI-HI (squares) and HI-CDW<sub>1</sub> (circles) critical points.  $L_m$  is the maximum length to extract  $\xi_e$  from a linear fit of  $\log(|E_+ - E_-|)$  versus  $L$  [84]. (c) Bulk gap  $\Delta E_{bulk} = E_1 - E_{GS}$  (orange) and charge gap  $\Delta E_{charge}$  (blue) for length  $L = 200$ . Decay of  $\mathcal{C}_1$  and  $\mathcal{O}_{1,x}^2$  (blue) and  $\mathcal{O}_{1,z}^2$  (green) obtained using iDMRG relative to: HI at  $V/J = 3.76$  (d), the HI-CDW<sub>1</sub> critical point at  $V/J = 3.86$  (e) and CDW<sub>1</sub> at  $V/J = 3.91$  (f). We employ a bond dimension  $D = 250$  and we cut the number of bosons per site at  $n_0 = 4$ .

tiferromagnetic order of CDW<sub>1</sub> is characterized by an exponential decay of  $\mathcal{O}_{1,x}^2$  but preserved long-range order of  $\mathcal{O}_{1,z}^2$ . Crucially, the CDW<sub>1</sub> has no topological features since, as discussed, its local magnetic order is captured by the two points correlation function

$$\mathcal{C}_1(|i-j|) = \langle S_1^z(i) S_1^z(j) \rangle. \quad (3)$$

In Figs. 1(d) and (f) we clearly see the expected behavior of eqs. (2) and (3) in the HI and CDW<sub>1</sub>. As discussed in [86], by varying  $V/J$  at intermediate values of  $U/J$ , a Gaussian and an Ising phase transition describing respectively the MI-HI and HI-CDW<sub>1</sub> critical points are found. As expected and confirmed by the diverging  $\xi_b$  shown in Fig. 1 (a), the bulk gap vanishes at these specific transition points, see Fig. 1 (c). The absence of a bulk gap may induce to think that localized edge modes also disappear. On the contrary, our calculations clearly demonstrate that this is not always the case. In particular, while at the Gaussian phase transition  $\xi_b^{-1}, \xi_e^{-1} = 0$ , at the HI-CDW<sub>1</sub> critical point the edge localization length remains finite in the thermodynamic limit. This proves the presence of localized edge modes formed by an empty site and a pair of bosons. Moreover, as reported in Fig. 1 (e), this critical point shows algebraic decay of both  $\mathcal{O}_{1,x}^2$  and  $\mathcal{C}_1$ . As discussed, this

algebraic decay does not take place in the HI, thus implying that a different topological phase exists at this critical point. It is now of great relevance to understand the origin of such TQCP. In this direction, our results in Fig. 1(c) show that a gap at energies higher than  $\Delta E_{bulk}$ , *i.e.* the charge gap  $\Delta E_{charge} = E_{GS}(N+1, L) + E_{GS}(N-1, L) - 2E_{GS}(N, L)$  counting for the effective magnetic ordering in both HI and  $CDW_{1/2}$ , does not vanish at the HI- $CDW_{1/2}$  transition point. This explains why at this TQCP, see Fig. 1 (e), we still find long-range order of uniquely a string correlator, namely  $\mathcal{O}_{1,z}^2$ , as required in SPT phases. As a consequence, it is natural to state that such high energy charge gap is the responsible for the protection of the edge states. It is worth to underline that this analysis can be used to interpret the physics of spin-1 chains where the same TQCP takes place [64]. In the latter case, a finite charge gap corresponds to a finite spin gap [39] and the string order parameter along the  $z$ -axis is still expected to be finite at criticality. As known [30, 31, 39, 87], for  $U = 0$  and truncated local Hilbert space to a maximum of two bosons per site, this homogeneous case is strictly equivalent to a spin-1 XXZ chain [88]. Interestingly, our results fully characterize a TQCP away from this spin-1 limit, thus generalizing the physics of TCPQs to new regimes of the extended Bose Hubbard model. Regardless, we believe that it is of great importance to explore whether similar TQCPs appear when effective spin-1 representations are not applicable.

*Dimerized case* ( $\delta J > 0$ ) at  $\bar{n} = 1/2$ . In this regime it has been demonstrated that for large enough  $U/J$  and intermediate  $V/J$ , a TMI appears [82]. The latter displays features analogous to the SPT phase appearing in the dimerized spin-1/2 Heisenberg model [89]. In Fig. 2(b) we show that the TMI hosts, as expected, localized edge modes signaled by a finite  $\xi_e$ . In this case, the edge states are given by either a vanishing or single occupation. Fig. 2(a) enlightens that a finite  $\Delta E_{bulk}$  [86] produces a finite bulk correlation length in the TMI phase. Moreover, our results in Fig. 2(d) show that the topological nature of TMI is captured by the long-range order of specific non-local string correlators

$$\mathcal{O}_{1/2,\alpha}^2(|i-j|) = \langle \mathcal{O}_{1/2,\alpha}(2i-1) \mathcal{O}_{1/2,\alpha}(2j) \rangle, \quad \alpha = x, z. \quad (4)$$

signaling non-local magnetic order between odd and even sites with alternated bosonic occupation. Here, the associated non-local order parameters are  $\mathcal{O}_{1/2,\alpha}(j) = e^{i\pi \sum_{k<j} S_{1/2}^\alpha(k)} S_{1/2}^\alpha(j)$  with  $S_{1/2}^z(i) = (1/2 - n_i)$  and  $S_{1/2}^x(i) = 1/2(\sqrt{1-n_i}b_i + b_i^\dagger \sqrt{1-n_i})$ . The topology results to be unstable for  $V < 0$ . In this regime, a diverging compressibility, obtained as the slope of  $\chi(\delta N) = (E(L/2 + \delta N) - E(L/2 - \delta N))/2\delta N$  with  $\delta N = \{1, 2\}$ , signals the presence of a first order phase transition where the system enters a regime of phase separation [86]. At this specific point we find that  $\xi_e^{-1}, \xi_b^{-1} = 0$ , meaning that the edge states disappear and the topology is destroyed. On the other hand, for larger NN repulsions the system undergoes a phase transition where the TMI is replaced by a trivial  $CDW_{1/2}$ , captured by the long-range order of the corresponding two points

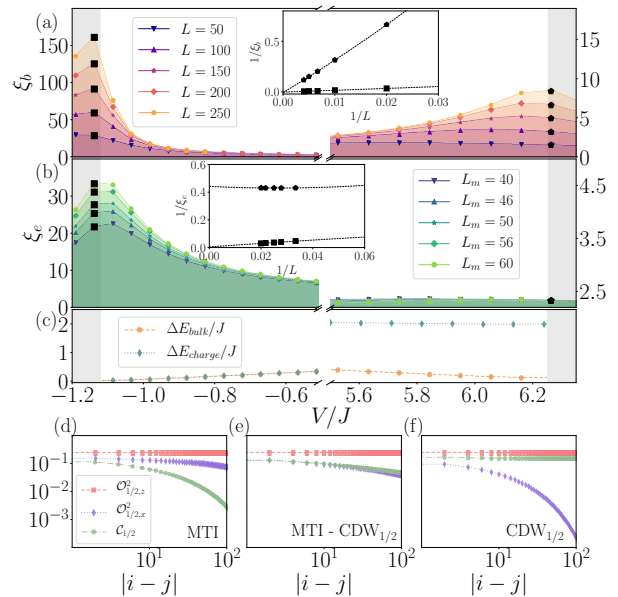


Figure 2. Edge  $\xi_e$  (a) and bulk  $\xi_b$  (b) correlation length in units of the lattice spacing  $a_{lat}$ , obtained using DMRG simulations of the model eq. (1) with  $\bar{n} = 1/2$ ,  $\delta J = 0.5$ ,  $U/J = 6$  as a function of  $V/J$ . The insets refer to the finite size extrapolation of  $\xi_e$  and  $\xi_b$  at the MI-HI (squares) and HI- $CDW_{1/2}$  (circles) critical points.  $L_m$  is the maximum length to extract  $\xi_e$  from a linear fit of  $\log(E_+ - E_-)$  versus  $L$  [84]. (c) Bulk gap  $\Delta E_{bulk} = E_1 - E_{GS}$  (orange) and charge gap  $\Delta E_{charge}$  (blue) for length  $L = 200$ . Decay of  $C_{1/2}$  (orange),  $\mathcal{O}_{1/2,x}^2$  (blue) and  $\mathcal{O}_{1/2,z}^2$  (green) obtained using iDMRG relative to: TMI at  $V/J = 6.03$  (d), the TMI- $CDW_{1/2}$  critical point at  $V/J = 6.35$  (e) and  $CDW_{1/2}$  at  $V/J = 6.97$  (f). We employ a bond dimension  $D = 250$  and we cut the number of bosons per site at  $n_0 = 3$ .

correlator

$$C_{1/2}(|i-j|) = \langle S_{1/2}^z(i) S_{1/2}^z(j) \rangle. \quad (5)$$

As in the previous case, TMI and  $CDW_{1/2}$  have respectively non-local and local antiferromagnetic order which now reflects the alternation between empty and singly occupied sites. In Fig. 2(a) we report that the critical point connecting the  $CDW_{1/2}$  and TMI is, as expected, signaled by a diverging  $\xi_b$ . This last point is therefore a consequence of the fact that here  $\Delta E_{bulk} = 0$ , see Fig. 2(c). Crucially, in Fig. 2(b) we see that localized edge states captured by a finite  $\xi_e$  remain stable at this transition point. As showed in Fig. 2(e), the latter is further characterized by an algebraic decay of  $\mathcal{O}_{1/2,x}^2$  and  $C_{1/2}$ . Therefore these results make evident that an effective lattice dimerization allows for the appearance of a TQCP. The latter is characterized by protected topological edge states formed by an empty and a single occupied state, thus different from the TQCP observed for  $\delta J = 0$ . On the other hand, the mechanism behind the TQCP for  $\delta J > 0$  is analogous to what we reported for the homogeneous case. Again, the topological nature of the critical point results to be captured by the long-range order of the  $z$ -oriented string correlator  $\mathcal{O}_{1/2,z}^2$ . More-

over, explicit calculations in Fig. 2(c) show that the charge gap reflecting the effective magnetism characterizing both TMI and  $CDW_{1/2}$  does not vanish at this transition point. Therefore this finite gap allows for the long-range of  $\mathcal{O}_{1/2,z}^2$  and thus for the survival of the topological edge states.

Relevantly, the results on the dimerized case provide a new example of a TQCP substantially different from the one found for  $\delta J = 0$ . More importantly, they also confirm the hypothesis that the two studied cases share a common mechanism as the responsible for the appearance of TQCPs. In particular, our results point in the direction that if two gapped phases, one topologically protected and the other trivial, are both characterized by a similar long-range order captured by a string correlator, as a consequence, the two phases are connected by a TQCP.

*Experimental realization and detection of a TQCP.* In this section we discuss how TQCPs could be observed using ultracold dysprosium atoms in an optical lattice. In addition to the usual contact interactions, the large magnetic dipole moment of  $10 \mu_B$ , where  $\mu_B$  denotes the Bohr magneton, makes such atoms interact highly non-locally through dipole-dipole repulsion. Since such interaction scales with the particle distance as  $1/r^3$ , it is necessary to trap the atoms in a lattice with short periodicity in order to achieve sizeable NN interactions  $V$ . Here a lattice formed using lasers with a wavelength of around 360 nm is particularly promising for this purpose [86]. The corresponding lattice spacing  $a_{lat} = 180$  nm results in a NN interaction strength of  $V/h \sim 200$  Hz, where  $h$  is Planck's constant. This is an enhancement by a factor of six compared to previous experiments with magnetic atoms [78] and a factor of four compared to experiments with dipolar molecules [90]. As shown in Fig. 3 and explained in details in [86], by changing the lattice depth  $V_0/E_R$  and directly tuning the onsite contact interaction between atoms using a Feshbach resonance [91, 92], it is possible to achieve values of interactions where TQCPs can be explored. This last point is proved by an explicit calculation of  $U_{i,j,k,l} = \int dx dx' w_i^*(x) w_j^*(x') V_{1D}(|x-x'|) w_k(x) w_l(x)$  where  $w_i(x)$  are the Gaussian approximation of localized Wannier functions and  $V_{1D}(|x-x'|)$  is a quasi-1D potential counting for the dipolar and  $s$ -wave interaction processes [93–95]. In this approximation the on-site and NN interaction are given by the integrals  $U = U_{i,i,i,i}$  and  $V = U_{i,i+1,i+1,i}$ . Notice that in 1D and for not too large  $V$ , dipolar interaction can neither produce new phases with respect to the case of NN interaction nor change the nature of the transition points. For this reason our cut of the dipolar interaction to NN turns out to be a very reliable approximation. Moreover, strongly-coupled bilayer geometries could be realized by implementing a sub-wavelength optical barrier inside the individual lattice sites of a one-dimensional lattice [96]. In this way an effective dimerization  $\delta J > 0$  can be achieved. Thanks to the strong dipolar interaction, we also estimate a critical temperature required to stabilize the topological phase on the order of tens of nK, well within the reach of current experiments. In such a setting, two-point density-density correlation functions  $\mathcal{C}_1$  and  $\mathcal{C}_{1/2}$ , string order parameters  $\mathcal{O}_{1,z}^2$  and  $\mathcal{O}_{1/2,z}^2$ , and edge correlation length  $\xi_e$  are directly accessible using quantum gas

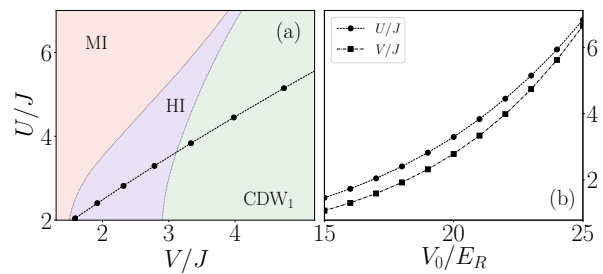


Figure 3. (a) Qualitative phase diagram of the extended Bose Hubbard model from eq. (1) at  $\delta J = 0$  and  $\bar{n} = 1$  [36]. The circles represent the examples of experimentally accessible values of the onsite interaction  $U/J$  and the NN repulsion  $V/J$  calculated by considering dysprosium atoms with dipole moment of  $10 \mu_B$  and  $s$ -wave scattering length  $a_{3D} = 91a_0$  with  $a_0$  the Bohr radius. The atoms are trapped in a lattice with longitudinal lattice spacing  $a_{lat} = 180$  nm and transverse confinement of frequency  $\omega_{\perp} = 2\pi \times 4$  kHz, see [86] for details. (b) Values of  $U/J$  (circles) and  $V/J$  (squares) calculated by considering lattice depth  $V_0/E_R$  ranging from 15 to 25. Notice that different choices of  $a_{3D}$  and  $\omega_{\perp}$  allow to achieve different sectors of the phase diagram.

microscopy [52, 97, 98]. However, the requirement of a short lattice wavelength poses a significant challenge for quantum gas microscopy, as the lattice wavelength is significantly below the Abbe resolution limit for the 421 nm imaging transition in dysprosium. As we show in detail [86], this limitation can be overcome by using super-resolution techniques to detect individual atoms below the diffraction limit. This scheme results to be inherently number resolving and can allow to individually image empty sites, as well as higher-order occupations, thus allowing for a complete characterization of TQCPs.

*Discussion and outlook* We have shown that the recently discovered phenomenon of topological phases occurring at quantum critical points can be explored in the celebrated extended Bose-Hubbard model. These phases turned out to be topological states with gapless bulk excitations but, at the same time, localized edge states. Our analysis has further revealed how different kinds of TQCPs can be found by adjusting the Hamiltonian parameters. Moreover, our results suggest the presence of a common mechanism to achieve TQCPs. In particular, we have showed that a TQCP takes place between two fully gapped phases, one topological and one trivial, when they are both characterized by a finite value of the same string correlator denoting a similar type of long-range order. In this scenario, we have demonstrated that, at criticality, a finite higher energy charge gap is able to protect the localized edge states. In order to provide a reliable route towards the experimental investigation of TQCPs, we have proposed a detailed experimental setup involving trapped dysprosium atoms at ultracold temperatures. Here, on one hand, laser beams producing short lattice spacing can be employed to achieve the desired region of the phase diagram and, on the other hand, a quantum gas microscope with super-resolution techniques can allow for an accurate detection of TQCPs.

Due to the fact that extended Bose-Hubbard Hamiltonians are of great relevance in different physical systems [99–103], we expect that our results can stimulate the study of TQCPs in a broad variety of research lines. Finally, as natural extensions of the present work, we believe that the investigation of TQCPs in fermionic systems, where the extra spin degrees of freedom can give rise to interesting topological states, might represent an intriguing topic. Moreover, we expect that the inspection of interesting Lattice Gauge Theories [104] where topological phases exist may reveal the presence of novel TQCPs.

*Acknowledgments* We thank A. Dauphin, A. Montorsi and G. Palumbo for discussion. J. F., D. G.-C., M. L. and L. B. acknowledge support from ERC AdG NOQIA, Spanish Ministry MINECO and State Research Agency AEI (“Severo Ochoa” Center of Excellence CEX2019-000910-S, Plan National FIDEUA PID2019-106901GB-I00/10.13039/501100011033, FPI), Fundació Cellex, Fundació Mir-Puig, Generalitat de Catalunya (AGAUR Grant No. 2017 SGR

1341, CERCA program, QuantumCAT U16-011424, co-funded by ERDF Operational Program of Catalonia 2014-2020), EU Horizon 2020 FET-OPEN OPTOLoGic (Grant No 899794) and the National Science Centre, Poland (Symfonia Grant No. 2016/20/W/ST4/00314), Marie Skłodowska-Curie grant STREDCH No 101029393, “La Caixa” Junior Leaders fellowships (ID100010434), and EU Horizon 2020 under Marie Skłodowska-Curie grant agreement No 847648 (LCF/BQ/PI19/11690013, LCF/BQ/PI20/11760031, LCF/BQ/PR20/11770012). T.L. acknowledges support from the Vector Stiftung and the European Research Council (ERC) under the European Union’s Horizon 2020 research and innovation programme (Grant agreement No. 949431). T.P. and T.L. acknowledge support by the German Research Foundation (DFG) within FOR2247 under Pf381/16-1 and Bu2247/1, Pf381/20-1, FUGG INST41/1056-1. We acknowledge QUANT:ERA collaborative project MAQS for financial support.

- 
- [1] M. Aorey, *Nature Physics* **12**, 616–618 (2016).  
 [2] N. Goldman, J. C. Budich, and P. Zoller, *Nature Physics* **12**, 639–645 (2016).  
 [3] T. Ozawa, H. M. Price, A. Amo, N. Goldman, M. Hafezi, L. Lu, M. C. Rechtsman, D. Schuster, J. Simon, O. Zilberberg, and I. Carusotto, *Rev. Mod. Phys.* **91**, 015006 (2019).  
 [4] X.-L. Qi and S.-C. Zhang, *Rev. Mod. Phys.* **83**, 1057 (2011).  
 [5] M. Z. Hasan and C. L. Kane, *Rev. Mod. Phys.* **82**, 3045 (2010).  
 [6] K. v. Klitzing, G. Dorda, and M. Pepper, *Phys. Rev. Lett.* **45**, 494 (1980).  
 [7] R. B. Laughlin, *Phys. Rev. B* **23**, 5632 (1981).  
 [8] D. J. Thouless, M. Kohmoto, M. P. Nightingale, and M. den Nijs, *Phys. Rev. Lett.* **49**, 405 (1982).  
 [9] N. Read and G. Moore, *Progress of Theoretical Physics Supplement* **107**, 157–166 (1992).  
 [10] D. C. Tsui, H. L. Stormer, and A. C. Gossard, *Phys. Rev. Lett.* **48**, 1559 (1982).  
 [11] R. B. Laughlin, *Phys. Rev. Lett.* **50**, 1395 (1983).  
 [12] W. P. Su and J. R. Schrieffer, *Phys. Rev. Lett.* **46**, 738 (1981).  
 [13] A. Kitaev, *Annals of Physics* **303**, 2–30 (2003).  
 [14] M. H. Freedman, *Proceedings of the National Academy of Sciences* **95**, 98 (1998).  
 [15] S. B. Bravyi and A. Y. Kitaev, arXiv preprint quant-ph/9811052 (1998).  
 [16] M. H. Freedman and D. A. Meyer, *Foundations of Computational Mathematics* **1**, 325 (2001).  
 [17] E. Dennis, A. Kitaev, A. Landahl, and J. Preskill, *Journal of Mathematical Physics* **43**, 4452–4505 (2002).  
 [18] A. Altland and M. R. Zirnbauer, *Phys. Rev. B* **55**, 1142 (1997).  
 [19] C. L. Kane and E. J. Mele, *Phys. Rev. Lett.* **95**, 146802 (2005).  
 [20] B. A. Bernevig and S.-C. Zhang, *Phys. Rev. Lett.* **96**, 106802 (2006).  
 [21] B. A. Bernevig, T. L. Hughes, and S.-C. Zhang, *Science* **314**, 1757–1761 (2006).  
 [22] A. P. Schnyder, S. Ryu, A. Furusaki, and A. W. W. Ludwig, *Phys. Rev. B* **78**, 195125 (2008).  
 [23] L. Fidkowski and A. Kitaev, *Phys. Rev. B* **83**, 075103 (2011).  
 [24] F. Pollmann, A. M. Turner, E. Berg, and M. Oshikawa, *Phys. Rev. B* **81**, 064439 (2010).  
 [25] Z.-C. Gu and X.-G. Wen, *Phys. Rev. B* **80**, 155131 (2009).  
 [26] X. Chen, Z.-C. Gu, Z.-X. Liu, and X.-G. Wen, *Science* **338**, 1604 (2012).  
 [27] A. Montorsi, F. Dolcini, R. C. Iotti, and F. Rossi, *Phys. Rev. B* **95**, 245108 (2017).  
 [28] F. D. M. Haldane, *Phys. Rev. Lett.* **50**, 1153 (1983).  
 [29] I. Affleck, T. Kennedy, E. H. Lieb, and H. Tasaki, *Phys. Rev. Lett.* **59**, 799 (1987).  
 [30] E. G. Dalla Torre, E. Berg, and E. Altman, *Phys. Rev. Lett.* **97**, 260401 (2006).  
 [31] E. Berg, E. G. Dalla Torre, T. Giamarchi, and E. Altman, *Phys. Rev. B* **77**, 245119 (2008).  
 [32] I. Nonne, P. Lecheminant, S. Capponi, G. Roux, and E. Boulat, *Phys. Rev. B* **81**, 020408 (2010).  
 [33] M. Dalmonte, M. Di Dio, L. Barbiero, and F. Ortolani, *Phys. Rev. B* **83**, 155110 (2011).  
 [34] X. Deng and L. Santos, *Phys. Rev. B* **84**, 085138 (2011).  
 [35] S. Furukawa, M. Sato, S. Onoda, and A. Furusaki, *Phys. Rev. B* **86**, 094417 (2012).  
 [36] D. Rossini and R. Fazio, *New Journal of Physics* **14**, 065012 (2012).  
 [37] K. Kobayashi, M. Okumura, Y. Ota, S. Yamada, and M. Machida, *Phys. Rev. Lett.* **109**, 235302 (2012).  
 [38] L. Barbiero, A. Montorsi, and M. Roncaglia, *Phys. Rev. B* **88**, 035109 (2013).  
 [39] S. Ejima and H. Fehske, *Phys. Rev. B* **91**, 045121 (2015).  
 [40] S. Fazzini, A. Montorsi, M. Roncaglia, and L. Barbiero, *New Journal of Physics* **19**, 123008 (2017).  
 [41] L. Barbiero, L. Dell’Anna, A. Trombettoni, and V. E. Korepin, *Phys. Rev. B* **96**, 180404 (2017).  
 [42] K. Kottmann, P. Huembeli, M. Lewenstein, and A. Acín, *Phys. Rev. Lett.* **125**, 170603 (2020).  
 [43] K. Kottmann, A. Haller, A. Acín, G. E. Astrakharchik, and M. Lewenstein, “Supersolid-superfluid phase separation in the extended bose-hubbard model,” (2021), arXiv:2106.05893 [cond-mat.quant-gas].  
 [44] S. R. Manmana, A. M. Essin, R. M. Noack, and V. Gurarie, *Phys. Rev. B* **86**, 205119 (2012).

- [45] J. Sirker, M. Maiti, N. P. Konstantinidis, and N. Sedlmayr, *Journal of Statistical Mechanics: Theory and Experiment* **2014**, P10032 (2014).
- [46] D. Wang, S. Xu, Y. Wang, and C. Wu, *Phys. Rev. B* **91**, 115118 (2015).
- [47] L. Barbiero, L. Santos, and N. Goldman, *Phys. Rev. B* **97**, 201115 (2018).
- [48] B. Sbierski and C. Karrasch, *Phys. Rev. B* **98**, 165101 (2018).
- [49] D. González-Cuadra, A. Dauphin, P. R. Grzybowski, P. Wójcik, M. Lewenstein, and A. Bermudez, *Phys. Rev. B* **99**, 045139 (2019).
- [50] D. González-Cuadra, A. Bermudez, P. R. Grzybowski, M. Lewenstein, and A. Dauphin, *Nature Communications* **10**, 2694 (2019).
- [51] X.-L. Yu, L. Jiang, Y.-M. Quan, T. Wu, Y. Chen, L.-J. Zou, and J. Wu, *Phys. Rev. B* **101**, 045422 (2020).
- [52] P. Sompet, S. Hirthe, D. Bourgund, T. Chalopin, J. Bibo, J. Koepsell, P. Bojović, R. Verresen, F. Pollmann, G. Salomon, C. Gross, T. A. Hilker, and I. Bloch, (2021), [arXiv:2103.10421 \[cond-mat.quant-gas\]](https://arxiv.org/abs/2103.10421).
- [53] S. de Léséleuc, V. Lienhard, P. Scholl, D. Barredo, S. Weber, N. Lang, H. P. Büchler, T. Lahaye, and A. Browaeys, *Science* **365**, 775 (2019).
- [54] J. P. Kestner, B. Wang, J. D. Sau, and S. Das Sarma, *Phys. Rev. B* **83**, 174409 (2011).
- [55] L. Fidkowski, R. M. Lutchyn, C. Nayak, and M. P. A. Fisher, *Phys. Rev. B* **84**, 195436 (2011).
- [56] J. D. Sau, B. I. Halperin, K. Flensberg, and S. Das Sarma, *Phys. Rev. B* **84**, 144509 (2011).
- [57] M. Cheng and H.-H. Tu, *Phys. Rev. B* **84**, 094503 (2011).
- [58] A. Keselman and E. Berg, *Phys. Rev. B* **91**, 235309 (2015).
- [59] T. Scaffidi, D. E. Parker, and R. Vasseur, *Phys. Rev. X* **7**, 041048 (2017).
- [60] J. Ruhman and E. Altman, *Phys. Rev. B* **96**, 085133 (2017).
- [61] D. E. Parker, T. Scaffidi, and R. Vasseur, *Phys. Rev. B* **97**, 165114 (2018).
- [62] R.-X. Zhang and C.-X. Liu, *Phys. Rev. Lett.* **120**, 156802 (2018).
- [63] R. Verresen, N. G. Jones, and F. Pollmann, *Phys. Rev. Lett.* **120**, 057001 (2018).
- [64] R. Verresen, R. Thorngren, N. G. Jones, and F. Pollmann, (2019), [arXiv:1905.06969 \[cond-mat.str-el\]](https://arxiv.org/abs/1905.06969).
- [65] S. Fazzini, L. Barbiero, and A. Montorsi, *Phys. Rev. Lett.* **122**, 106402 (2019).
- [66] A. Montorsi, S. Fazzini, and L. Barbiero, *Phys. Rev. A* **101**, 043618 (2020).
- [67] S. R. White, *Phys. Rev. Lett.* **69**, 2863 (1992).
- [68] U. Schollwöck, *Annals of Physics* **326**, 96–192 (2011).
- [69] J. Hauschild and F. Pollmann, *SciPost Phys. Lect. Notes* **5** (2018), code available from <https://github.com/tenpy/tenpy>, [arXiv:1805.00055](https://arxiv.org/abs/1805.00055).
- [70] T. Lahaye, C. Menotti, L. Santos, M. Lewenstein, and T. Pfau, *Reports on Progress in Physics* **72**, 126401 (2009).
- [71] M. Schmitt, M. Wenzel, F. Böttcher, I. Ferrier-Barbut, and T. Pfau, *Nature* **539**, 259–262 (2016).
- [72] L. Chomaz, S. Baier, D. Petter, M. J. Mark, F. Wächtler, L. Santos, and F. Ferlaino, *Phys. Rev. X* **6**, 041039 (2016).
- [73] Y. Tang, W. Kao, K.-Y. Li, S. Seo, K. Mallayya, M. Rigol, S. Gopalakrishnan, and B. L. Lev, *Phys. Rev. X* **8**, 021030 (2018).
- [74] M. Guo, F. Böttcher, J. Hertkorn, J.-N. Schmidt, M. Wenzel, H. P. Büchler, T. Langen, and T. Pfau, *Nature* **574**, 386–389 (2019).
- [75] L. Tanzi, S. M. Rocuzzo, E. Lucioni, F. Famà, A. Fioretti, C. Gabbanini, G. Modugno, A. Recati, and S. Stringari, *Nature* **574**, 382–385 (2019).
- [76] L. Chomaz, D. Petter, P. Ilzhöfer, G. Natale, A. Trautmann, C. Politi, G. Durastante, R. M. W. van Bijnen, A. Patscheider, M. Sohmen, M. J. Mark, and F. Ferlaino, *Phys. Rev. X* **9**, 021012 (2019).
- [77] W. Kao, K.-Y. Li, K.-Y. Lin, S. Gopalakrishnan, and B. L. Lev, *Science* **371**, 296 (2021).
- [78] S. Baier, M. J. Mark, D. Petter, K. Aikawa, L. Chomaz, Z. Cai, M. Baranov, P. Zoller, and F. Ferlaino, *Science* **352**, 201 (2016).
- [79] T. D. Kühner and H. Monien, *Phys. Rev. B* **58**, R14741 (1998).
- [80] T. D. Kühner, S. R. White, and H. Monien, *Phys. Rev. B* **61**, 12474 (2000).
- [81] F. Grusdt, M. Hönig, and M. Fleischhauer, *Phys. Rev. Lett.* **110**, 260405 (2013).
- [82] K. Sugimoto, S. Ejima, F. Lange, and H. Fehske, *Phys. Rev. A* **99**, 012122 (2019).
- [83] W. P. Su, J. R. Schrieffer, and A. J. Heeger, *Phys. Rev. Lett.* **42**, 1698 (1979).
- [84] We extract  $-1/\xi_e(L)$  from the slope of the linear fit  $\log(|E_+ - E_-|)$  versus  $L$ , where we take values of  $L$  from the interval  $[L_m - 30, L_m]$  (Fig.1) and  $[L_m - 10, L_m]$  (Fig.2). We assume that the edge correlation length  $\xi_e(L)$  is constant within the interval.
- [85] In order to select the  $|L\rangle/|R\rangle$  configurations for the computation of the edge correlation length  $\xi_e$ , we fix the edge occupation by adding local chemical potentials at the edges with opposite sign.
- [86] See Supplementary material.
- [87] X. Deng, R. Citro, E. Orignac, A. Minguzzi, and L. Santos, *New Journal of Physics* **15**, 045023 (2013).
- [88] The condition  $\bar{n} = 1$  translates into  $S_{tot}^z = 0$  when considering spin-1 systems. By using the relation  $S_{i,1}^z = 1 - n_i$ , one can derive that  $\Delta E_{charge} = E_{GS}(S_{tot}^z = -1) + E_{GS}(S_{tot}^z = 1) - 2E_{GS}(S_{tot}^z = 0)$  which is the usual definition of spin gap [26].
- [89] T. W. Wang, B. Li, and S. Y. Cho, *Phys. Rev. B* **87**, 054402 (2013).
- [90] B. Yan, S. A. Moses, B. Gadway, J. P. Covey, K. R. A. Hazard, A. M. Rey, D. S. Jin, and J. Ye, *Nature* **501**, 521 (2013).
- [91] E. Lucioni, L. Tanzi, A. Fregosi, J. Catani, S. Gozzini, M. Inguscio, A. Fioretti, C. Gabbanini, and G. Modugno, *Phys. Rev. A* **97**, 060701 (2018).
- [92] J.-N. Schmidt, J. Hertkorn, M. Guo, F. Böttcher, M. Schmidt, K. Ng, S. Graham, T. Langen, M. Zwierlein, and T. Pfau, *Physical Review Letters* **126** (2021), [10.1103/physrevlett.126.193002](https://doi.org/10.1103/physrevlett.126.193002).
- [93] S. Sinha and L. Santos, *Phys. Rev. Lett.* **99**, 140406 (2007).
- [94] F. Deuretzbacher, J. C. Cremon, and S. M. Reimann, *Phys. Rev. A* **81**, 063616 (2010).
- [95] N. Bartolo, D. J. Papoular, L. Barbiero, C. Menotti, and A. Recati, *Phys. Rev. A* **88**, 023603 (2013).
- [96] M. Lacki, M. A. Baranov, H. Pichler, and P. Zoller, *Phys. Rev. Lett.* **117**, 233001 (2016).
- [97] M. Endres, M. Cheneau, T. Fukuhara, C. Weitenberg, P. Schauß, C. Gross, L. Mazza, M. C. Bañuls, L. Pollet, I. Bloch, and S. Kuhr, *Science* **334**, 200 (2011).
- [98] T. A. Hilker, G. Salomon, F. Grusdt, A. Omran, M. Boll, E. Demler, I. Bloch, and C. Gross, *Science* **357**, 484 (2017).
- [99] C. Bruder, R. Fazio, and G. Schön, *Annalen der Physik* **14**, 566 (2005).

- [100] T. Giamarchi, C. Rüegg, and O. Tchernyshyov, *Nature Physics* **4**, 198–204 (2008).
- [101] R. Landig, L. Hruby, N. Dogra, M. Landini, R. Mottl, T. Donner, and T. Esslinger, *Nature* **532**, 476–479 (2016).
- [102] S. Asban and S. Mukamel, *Phys. Rev. Lett.* **123**, 260502 (2019).
- [103] P. Karpov and F. Piazza, “Light-induced quantum droplet phases of lattice bosons in multimode cavities,” (2021), [arXiv:2106.13226 \[cond-mat.quant-gas\]](https://arxiv.org/abs/2106.13226).
- [104] Y. Kuno, S. Sakane, K. Kasamatsu, I. Ichinose, and T. Matsui, *Phys. Rev. D* **95**, 094507 (2017).

# Supplementary Material for: *Topological quantum critical points in the extended Bose-Hubbard model*

Joana Fraxanet,<sup>1</sup> Daniel González-Cuadra,<sup>1</sup> Tilman Pfau,<sup>2</sup> Maciej Lewenstein,<sup>1,3</sup> Tim Langen,<sup>2</sup> and Luca Barbiero<sup>1</sup>

<sup>1</sup>ICFO - Institut de Ciències Fotòniques, The Barcelona Institute of Science and Technology, 08860 Castelldefels (Barcelona), Spain

<sup>2</sup>5. Physikalisches Institut and Center for Integrated Quantum Science and Technology, Universität Stuttgart, Pfaffenwaldring 57, 70569 Stuttgart, Germany

<sup>3</sup>ICREA, Pg. Lluís Companys 23, ES-08010 Barcelona, Spain

(Dated: June 30, 2021)

*a. Phase diagram of the homogeneous case ( $\delta J = 0$ ) at  $\bar{n} = 1$ .* The homogeneous case at unit density displays three fully gapped phases for relatively large  $U/J$ . As shown in Fig. 1, the first encountered phase is a Mott insulator occurring at small  $V/J$ . The uniform particle distribution peculiar of this Mott phases is captured by the long-range behavior of the parity correlator  $\mathcal{P}(j) = e^{i\pi \sum_{k < j} S_k^z}$  [1]. This last aspect reflects the absence of any kind of effective magnetic order in MI. A further increase of the NN repulsion allows the system to enter in the SPT Haldane insulator. Due to its topological nature, HI uniquely shows long-range order of string order parameters  $\mathcal{O}_{1,z}^2$  and  $\mathcal{O}_{1,x}^2$ . The long-range order of the string  $\mathcal{O}_{1,z}^2$  also reflects the hidden, or equivalently non-local, effective antiferromagnetic order existing between pairs and empty sites. For larger  $V/J$  an Ising phase transition where  $\Delta E_{bulk} = 0$  occurs. As a consequence, at this specific point  $\mathcal{O}_{1,x}^2$  and  $\mathcal{C}_1$  go to zero algebraically. Crucially, here the charge gap remains finite and, as we show in Fig. 1, it allows to  $\mathcal{O}_{1,z}^2$  to have long-range order which leads to a topological quantum critical point with localized edge states. In the large  $V/J$  regime the topological order is replaced by a trivial charge density wave state  $CDW_1$ . Here, the effective local antiferromagnetic order between pairs and empty sites is captured by the long-range

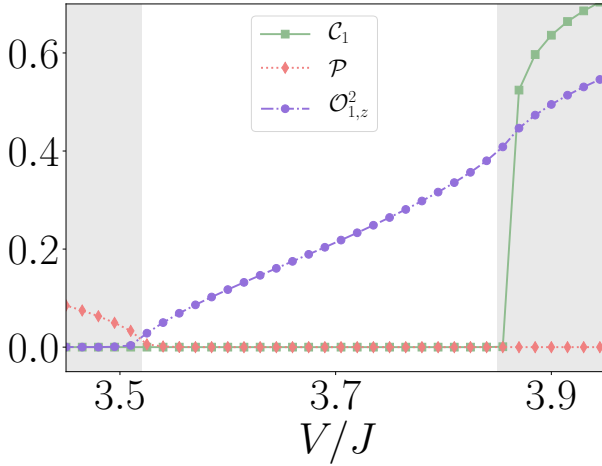


Figure 1:  $\mathcal{C}_1$  (green), parity  $\mathcal{P}$  (magenta) and  $\mathcal{O}_{1,z}^2$  (purple) for  $|i-j| = 200$ ,  $U/J = 6$ ,  $\delta J = 0$  and  $\bar{n} = 1$ . In the iDMRG calculations we consider a unit cell of  $L = 4$  bond dimension  $BD = 250$  and maximum number of bosons per site at  $n_0 = 4$ .

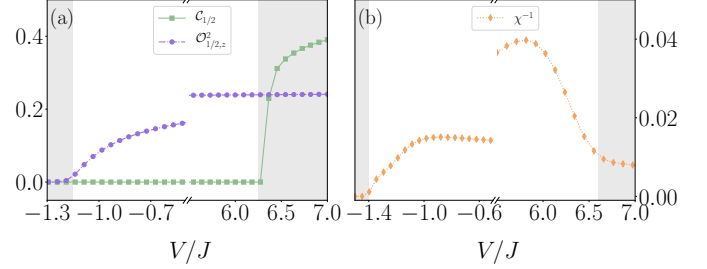


Figure 2: (a)  $\mathcal{C}_{1/2}$  and  $\mathcal{O}_{1/2,z}^2$  for  $|i-j| = 200$ ,  $U/J = 6$ ,  $\delta J = 0.5$  and  $\bar{n} = 1/2$  using iDMRG with bond dimension  $BD = 250$ . (b) Inverse compressibility  $\chi^{-1}$  for  $U/J = 6$ ,  $\delta J = 0.5$ ,  $\bar{n} = 1/2$  and  $L = 200$  using DMRG simulations with bond dimension  $BD = 200$ . In both cases, we consider a maximum number of bosons per site  $n_0 = 3$ .

order of  $\mathcal{C}_1$  but at the same time it allows for  $\mathcal{O}_{1,z}^2 \neq 0$ .

*b. Phase diagram of the dimerized case ( $\delta J > 0$ ) at  $\bar{n} = 1/2$ .* In analogy with the previous case, a large on-site repulsion allows for three different phases, see Fig. 2 (a). As we show in Fig. 2 (b), for attractive NN interaction a gapless regime of phase separation with infinite compressibility  $\chi$  appears. By increasing  $V$ , a first order phase transition, where  $\Delta E_{bulk} = \Delta E_{charge} = 0$  (as shown in Fig. 2 of the main text), signals the appearance of a topological Mott insulator (TMI) with non-local magnetic order between singly occupied and empty sites. The latter is characterized by long-range order of string correlators  $\mathcal{O}_{1/2,z}^2$  and  $\mathcal{O}_{1/2,x}^2$ . The TMI results unstable for larger NN repulsions. As shown in Fig. 2 (a) in this regime, where the locally magnetic  $CDW_{1/2}$  represents the ground state order, long-range of  $\mathcal{C}_{1/2}$  is found. At the TMI- $CDW_{1/2}$  transition point, we find that  $\Delta E_{bulk} = 0$  and  $\Delta E_{charge} \neq 0$ . In analogy with the  $\delta J = 0$  case, the long-range order of  $\mathcal{O}_{1/2,z}^2$  and the algebraically vanishing  $\mathcal{O}_{1/2,x}^2$  and  $\mathcal{C}_{1/2}$  allow to classify this transition point as a TQCP.

*c. Interaction parameters for dysprosium atoms with short inter-site spacing.* Here we propose an experimental setup which should allow to explore TQCPs. Our scheme is based on  $^{164}\text{Dy}$  atoms with a magnetic dipole moment of  $10 \mu_B$ , where  $\mu_B$  is the Bohr magneton. The atoms are trapped in a one-dimensional optical lattice with very short inter-site spacing  $a_{lat} = 180 \text{ nm}$ . The choice of such a short lattice spacing allows to explore and later probe a large portion of the extended Bose-Hubbard model phase diagram characterized by the presence of TQCPs. In order to prove this point

one has to calculate the following integral:

$$U_{i,j,k,l} = \int dx dx' w_i^*(x) w_j^*(x') V_{1D}(|x-x'|) w_k(x') w_l(x) \quad (1)$$

where  $w_i(x)$  are localized wannier functions which can be approximated by Gaussian functions with a width given by  $2E_R\sqrt{s}/\hbar$ , where  $s = V_0/E_R$  characterizes the depth of the lattice. By considering strong transverse confinement frequencies,  $\omega_\perp = 2\pi \times 4$  kHz in our case, the interaction potential eq. (1) can be derived upon considering Gaussian wave functions along the the transverse directions  $y, z$  and dipoles pointing perpendicularly to the longitudinal lattice  $x$ -direction. In this limit, as shown in [2–5], the quasi one-dimensional interacting potential takes the form

$$V_{1D}(|x-x'|) = \left( g_{1D} - \frac{2\hbar^2 r^*}{3ml_\perp^2} \right) \delta(|x-x'|) + \frac{\hbar^2 r^*}{ml_\perp^3} \left[ \sqrt{\frac{\pi}{8}} e^{-\frac{|x-x'|^2}{l_\perp^2}} \left( \frac{|x-x'|^2}{l_\perp^2} + 1 \right) \text{Erfc} \left( \frac{|x-x'|}{l_\perp\sqrt{2}} \right) - \frac{|x-x'|}{2l_\perp} \right] \quad (2)$$

where energies and lengths are expressed in unit of laser recoil energy  $E_R = \pi^2 \hbar^2 / 2ma_{lat}^2$  and  $a_{lat}$  respectively. Moreover,  $r^* = m\mu_0\mu^2 / 4\pi\hbar^2$  denotes the usually called dipolar length and  $l_\perp = (\hbar/m\omega_\perp)^{1/2}$  is the harmonic oscillator length of the transversal confinement. The latter can be created using a second, weaker optical lattice in the transversal direction. Note that in order to avoid long-range dipolar coupling of neighboring 1D systems, all but a single one need to be removed during the preparation. While the second line in eq. (2) describes the non-local tail of the interaction, it is worth to underline that the first line takes into account the overall contact repulsion produced by both the dipolar interaction and the  $s$ -wave scattering processes  $g_{1D} = 2\hbar^2 a_{3D} / ml_\perp^2$  where  $a_{3D} = 91a_0$  and  $a_0$  is the Bohr radius. As shown in the main text the range of parameters  $U = U_{i,i,i,i}$  and  $V = U_{i,i+1,i+1,i}$  where TQCPs have been predicted to appear can be easily reached.

*d. Detection of TQCPs using quantum gas microscopy.* As mentioned in the main text, a quantum gas microscope represents the most powerful and efficient experimental techniques to detect quantum phases of matter and specifically TQCPs. However, the requirement of a short lattice wavelength poses a significant challenge for quantum gas microscopy, as the lattice wavelength is significantly below the Abbe resolution limit for the 421 nm imaging transition in dysprosium. As schematically shown in Fig.3, this limitation can be overcome by using super-resolution techniques to detect individual atoms below the diffraction limit. So

far, super-resolution microscopy of cold atoms has been realized using two different techniques for caesium [6] and ytterbium [7]. These techniques both achieve a spatial resolution of a few tens of nanometers and rely on the nonlinear response of the atoms to an optical pumping pulse and coupling to a dark state, respectively. In dysprosium, super-resolution microscopy can be realized using a shelving approach that exploits the narrow 1001 nm transition from the ground-state to a long-lived excited state [8]. The principle of this technique is outlined in Fig. 3. Starting from a frozen atomic distribution in a deep lattice, the majority of atoms are transferred to a long-lived excited state, and only the atoms left in the ground state are imaged. The latter can be realized using fast standard imaging on the broad 421 nm transition, with a linewidth of  $\Gamma = 2\pi \times 32.5$  MHz. Subsequently, the excited atoms are returned to the ground state and imaged as well. In this process, working at a magic wavelength close to 360 nm, and consequently  $a_{lat} = 180$  nm, assures that the lattice potential is the same for the ground and the long-lived excited state in dysprosium [9, 10]. We note that this technique is conceptually closely related to stochastic optical reconstruction microscopy (STORM), which is widely used in biology and life sciences [11].

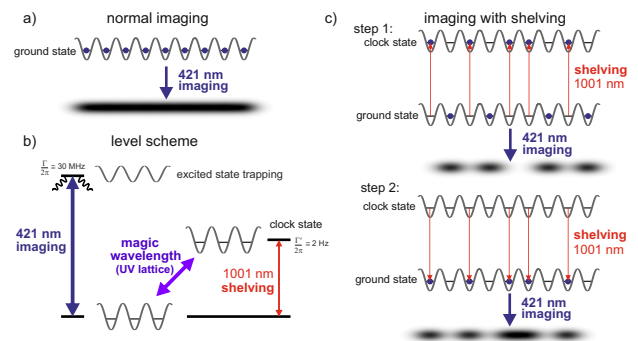


Figure 3: Shelving imaging of dysprosium atoms trapped in a short wavelength optical lattice. (a) Imaging the atoms with standard imaging at a wavelength of 421 nm will not suffice to reach single site resolution. (b) Energy levels in dysprosium allow for simultaneous magic wavelength trapping and narrow-line transitions [8], which can be used as a shelving transition. (c) Working principle of the shelving technique: In a first step around half of the atoms are pumped to the long-lived excited state and the remaining atoms are imaged. In a second step the atoms from the excited state are pumped down to the ground state again and imaged subsequently. Splitting the process into more steps, for example using a superlattice, will further improve the resolution.

- [1] E. Berg, E. G. Dalla Torre, T. Giamarchi, and E. Altman, Phys. Rev. B **77**, 245119 (2008).  
 [2] S. Sinha and L. Santos, Phys. Rev. Lett. **99**, 140406 (2007).  
 [3] F. Deuretzbacher, J. C. Cremon, and S. M. Reimann, Phys. Rev. A **81**, 063616 (2010).  
 [4] F. Deuretzbacher, J. C. Cremon, and S. M. Reimann, Phys. Rev.

- A **87**, 039903 (2013).  
 [5] N. Bartolo, D. J. Papoular, L. Barbiero, C. Menotti, and A. Recati, Phys. Rev. A **88**, 023603 (2013).  
 [6] M. McDonald, J. Trisnadi, K.-X. Yao, and C. Chin, Phys. Rev. X **9**, 021001 (2019).  
 [7] S. Subhankar, Y. Wang, T.-C. Tsui, S. L. Rolston, and J. V.

- Porto, Phys. Rev. X **9**, 021002 (2019).
- [8] N. Petersen, M. Trümper, and P. Windpassinger, Phys. Rev. A **101**, 042502 (2020).
- [9] H. Li, J.-F. Wyart, O. Dulieu, S. Nascimbène, and M. Lepers, Journal of Physics B: Atomic, Molecular and Optical Physics **50**, 014005 (2016).
- [10] M. Lepers, private communication.
- [11] B. Huang, W. Wang, M. Bates, and X. Zhuang, Science **319**, 810 (2008).